Research Article | Vol. 26, No. 10 | 14 May 2018 | OPTICS EXPRESS 13311
Optics EXPRESS

Novel fabrication technique for phase-shifted fiber Bragg gratings using a variable-velocity scanning beam and a shielded phase mask

JIANGTAO ZHOU,[1,2,3] KUIKUI GUO,[1,3] JUN HE,[1,*] MAOXIANG HOU,[1] ZHE ZHANG,[1] CHANGRUI LIAO,[1] YING WANG,[1] GAIXIA XU,[1] AND YIPING WANG[1]

[1]*Key Laboratory of Optoelectronic Devices and Systems of Ministry of Education and Guangdong Province, College of Optoelectronic Engineering, Shenzhen University, Shenzhen 518060, China*
[2]*Laboratory of Physics of Living Matter, Ecole Polytechnique Fédérale de Lausanne (EPFL), Lausanne 1015, Switzerland*
[3]*These authors contributed equally to this work*
[*]*hejun07@szu.edu.cn*

Abstract: A new method is proposed and demonstrated for fabricating phase-shifted fiber Bragg gratings (FBGs) using a variable-velocity scanning UV laser beam in combination with a shielded phase mask. The transmission properties of phase-shifted FBGs were analyzed based on coupled-mode theory and a transfer matrix method. The grating is divided into three parts to allow for easier analysis of FBG properties. These segments included a uniform FBG1 and FBG2 which were separated by a shielded section. A novel phase-shifted FBG was fabricated using this method, in which the refractive indices of FBG1 and FBG2 were different. Transmission properties of these phase-shifted FBGs were simulated numerically using MATLAB, and the experimental results and simulated results are in good agreement. In addition to the length and effective refractive index of the shielded section, the phase shift value of a phase-shifted FBG was also found to be dependent on the lengths and effective refractive indices of FBG1 and FBG2. Moreover, we predicted that changing the scanning velocity for fabricating FBG2 would adjust phase shift value, which exhibits a positive linear relationship with the scanning velocity. These results can provide guidelines for fabricating any phase shift value FBGs. This technique is simple, convenient, and may be developed further for use in fabricating novel tunable fiber filters or DFB fiber lasers.

OCIS codes: (060.3735) Fiber Bragg gratings; (350.2770) Gratings; (050.5080) Phase shift; (120.2440) Filters.

References and links

1. A. A. S. Falah, M. R. Mokhtar, Z. Yusoff, and M. Ibsen, "Reconfigurable phase-shifted fiber Bragg grating using localized micro-strain," IEEE Photonics Technol. Lett. **28**(9), 951–954 (2016).
2. X. Zhou, Y. Dai, J. M. Karanja, F. Liu, and M. Yang, "Fabricating phase-shifted fiber Bragg grating by simple postprocessing using femtosecond laser," Opt. Eng. **56**(2), 027108 (2017).
3. G. P. Agrawal and S. Radic, "Phase-shifted fiber Bragg gratings and their application for wavelength demultiplexing," IEEE Photonics Technol. Lett. **6**(8), 995–997 (1994).
4. X. Zou, M. Li, W. Pan, L. Yan, J. Azaña, and J. Yao, "All-fiber optical filter with an ultranarrow and rectangular spectral response," Opt. Lett. **38**(16), 3096–3098 (2013).
5. are B. Lin, M. Jiang, S. C. Tjin, and P. Shum, "Tunable microwave generation using a phase-shifted chirped fiber Bragg grating," IEEE Photonics Technol. Lett. **23**(18), 1292–1294 (2011).
6. W. Li, M. Li, and J. Yao, "A narrow-passband and frequency-tunable microwave photonic filter based on phase-modulation to intensity-modulation conversion using a phase-shifted fiber Bragg grating," IEEE Trans. Microw. Theory Tech. **60**(5), 1287–1296 (2012).
7. M. Li, N. Huang, N. Zhu, and Y. Deng, "Ka-band tunable flat-top microwave photonic filter using a multi-phase-shifted fiber Bragg grating," IEEE Photonics J. **6**(4), 1–8 (2014).
8. H. Qi, Z. Song, S. Li, J. Guo, C. Wang, and G. D. Peng, "Apodized distributed feedback fiber laser with asymmetrical outputs for multiplexed sensing applications," Opt. Express **21**(9), 11309–11314 (2013).
9. M. Li, X. Chen, T. Fujii, Y. Kudo, H. Li, and Y. Painchaud, "Multiwavelength fiber laser based on the utilization of a phase-shifted phase-only sampled fiber Bragg grating," Opt. Lett. **34**(11), 1717–1719 (2009).
10. D. Gatti, G. Galzerano, D. Janner, S. Longhi, and P. Laporta, "Fiber strain sensor based on a pi-phase-shifted Bragg grating and the pound-drever-hall technique," Opt. Express **16**(3), 1945–1950 (2008).

#326584 https://doi.org/10.1364/OE.26.013311
Journal © 2018 Received 21 Mar 2018; revised 22 Apr 2018; accepted 26 Apr 2018; published 8 May 2018

11. F. Zhu, Z. Zhang, C. Liao, Y. Wang, L. Xu, J. He, C. Wang, Z. Li, T. Yang, and Y. Wang, "Taper embedded phase-shifted fiber Bragg grating fabricated by femtosecond laser line-by-line inscription," IEEE Photonics J. **9**(6), 1–8 (2017).
12. A. Rosenthal, D. Razansky, and V. Ntziachristos, "High-sensitivity compact ultrasonic detector based on a pi-phase-shifted fiber Bragg grating," Opt. Lett. **36**(10), 1833–1835 (2011).
13. C. Liao, L. Xu, C. Wang, D. N. Wang, Y. Wang, Q. Wang, K. Yang, Z. Li, X. Zhong, J. Zhou, and Y. Liu, "Tunable phase-shifted fiber Bragg grating based on femtosecond laser fabricated in-grating bubble," Opt. Lett. **38**(21), 4473–4476 (2013).
14. S. Legoubin, E. Fertein, M. Douay, P. Bernage, P. Niay, F. Bayon, and T. Georges, "Formation of moire grating in core of germanosilicate fiber by transverse holographic double exposure method," Electron. Lett. **27**(21), 1945–1947 (1991).
15. W. H. Loh, M. J. Cole, M. N. Zervas, S. Barcelos, and R. I. Laming, "Complex grating structures with uniform phase masks based on the moving fiber-scanning beam technique," Opt. Lett. **20**(20), 2051–2053 (1995).
16. S. Rota-Rodrigo, L. Rodriguez-Cobo, M. A. Quintela, J. M. Lopez-Higuera, and M. Lopez-Amo, "Dual-wavelength single-longitudinal mode fiber laser using phase-shift Bragg gratings," IEEE J. Sel. Top. Quantum Electron. **20**(5), 161–165 (2014).
17. J. He, Y. Wang, C. Liao, Q. Wang, K. Yang, B. Sun, G. Yin, S. Liu, J. Zhou, and J. Zhao, "Highly birefringent phase-shifted fiber Bragg gratings inscribed with femtosecond laser," Opt. Lett. **40**(9), 2008–2011 (2015).
18. E. Chehura, S. W. James, and R. P. Tatam, "A simple and wavelength-flexible procedure for fabricating phase-shifted fiber Bragg gratings," Meas. Sci. Technol. **21**(9), 212–216 (2010).
19. Q. Li, F. Yan, W. Peng, T. Feng, S. Feng, S. Tan, P. Liu, and W. Ren, "DFB laser based on single mode large effective area heavy concentration EDF," Opt. Express **20**(21), 23684–23689 (2012).
20. K. Yelen, L. M. B. Hickey, and M. N. Zervas, "A new design approach for fiber DFB lasers with improved efficiency," IEEE J. Quantum Electron. **40**(6), 711–720 (2004).
21. M. Yamada and K. Sakuda, "Analysis of almost-periodic distributed feedback slab waveguides via a fundamental matrix approach," Appl. Opt. **26**(16), 3474–3478 (1987).
22. T. Erdogan, "Fiber grating spectra," J. Lightwave Technol. **15**(8), 1277–1294 (1997).
23. L. Wei and J. W. Y. Lit, "Phase-shifted Bragg grating filters with symmetrical structures," J. Lightwave Technol. **15**(8), 1405–1410 (1997).
24. M. A. Rodriguez, M. S. Malcuit, and J. J. Butler, "Transmission properties of refractive index-shifted Bragg gratings," Opt. Commun. **177**(1), 251–257 (2000).
25. Y. O. Barmenkov, D. Zalvidea, S. Torres-Peiró, J. L. Cruz, and M. V. Andrés, "Effective length of short Fabry-Perot cavity formed by uniform fiber Bragg gratings," Opt. Express **14**(14), 6394–6399 (2006).
26. Y. Zhang, B. O. Guan, and H. Y. Tam, "Characteristics of the distributed Bragg reflector fiber laser sensor for lateral force measurement," Opt. Commun. **281**(18), 4619–4622 (2008).

1. Introduction

The phase-shifted fiber Bragg gratings (FBGs) are currently of significant interest to researchers due to their inherent advantages, such as flexibility, immunity to electromagnetic interference, and small size [1]. Phase-shifted FBGs exhibit a characteristic of narrow transmission window as a type of band-pass filter [2]. Hence, they are widely used in many applications such as dense wavelength-division-multiplexing (DWDM) [3,4], high-fineness tunable optical filters [5–7], and distributed feedback (DFB) fiber lasers [8,9]. Moreover, they have also been used as high performance sensors for measuring strain [10,11], ultrasonic signal [12], liquid refractive index [13], and critical metrics in several other fields. Over the past decade, an extensive variety of methods have been reported for phase-shifted FBG fabrication, such as Moire method [14], moving fiber-scanning beam method [8,15], and shielded phase mask method [16], Other techniques have included the creation of internal micro-structures [13], overexposure to a near-infrared femtosecond laser with a uniform phase mask [17]. However, these methods have specific disadvantages as detailed in the comparison of phase-shifted FBG fabrication methods presented by Chehura *et al* [18]. These methods feature fabrication limitations, such as complex systems, poor tolerance, insufficient repeatability, and high processing time.

The scanning beam technique coupled with a phase mask is more reliable for fabricating long phase-shifted FBGs and includes fewer defects than other preparation methods. Uniform long phase-shifted FBGs with the length of several centimeters could be fabricated using this method. This type of phase-shifted FBGs typically has a narrow transmission peak in the stop band and hence is particularly suitable for use as a band-pass optical filter. One previous study produced a π-phase-shifted grating using the moving fiber-scanning beam method

Optics EXPRESS

combined with a computer-controlled piezoelectric transducer (PZT) stage [15]. However, this approach encountered difficulties in accurately controlling the relative shift between the fiber and the phase mask. Another study reported on a procedure for fabricating phase-shifted FBGs based on a two-beam interferometer and a fiber translation. However, the resulting phase-shifted FBG exhibited a relatively wide transmission passband (i.e. ~82 pm FWHM) [18]. In 2014, Sergio *et al* demonstrated a new type of phase-shifted superstructure FBG which was inscribed into the optical fiber by opening and closing the laser shutter at preset locations [16]. This method suffered from a complex design and fabrication process.

Conventional phase-shifted FBGs include common features which contain two identical effective refractive index gratings and a phase-shifted section. However, in some specific applications, such as high performance DFB fiber lasers, asymmetric designs in the phase-shifted FBGs would benefit for improving the laser efficiency. The asymmetric phase-shifted FBGs structures include using different length proportion [19] or using different refractive index modulation depths [20] on the left and right gratings. Unfortunately, high quality long phase-shifted FBGs which include two different effective refractive index gratings are less common and lacking in the current literature.

In this paper, we proposed a new method for fabricating unique phase-shifted FBGs using a scanning UV laser beam together with a shielded phase mask. Unlike methods reported previously, the presented phase-shifted FBG was fabricated using a variable-velocity scanning technique. The phase shift value can be modified by changing the scanning velocity, which exhibits a positive linear relationship between the phase shift value and the scanning velocity. In the first stage, an ordinary uniform FBG1 was inscribed using the scanning velocity v_1, as shown in Fig. 1. The transmission properties of this uniform FBG1 were then simulated numerically in MATLAB using a model based on coupled-mode theory [21] and the transfer matrix method [22]. The uniform FBG1 transmission evolution spectra were consistent with the simulated results. In the second stage, a plate was positioned in front of the phase mask and used to shield the laser to generate unexposed region during the scanning process. Lastly, the uniform FBG2 was fabricated using the scanning velocity v_2. During this time, the transmission spectra evolved gradually from the original FBG to a phase-shifted FBG. These phase-shifted FBGs transmission spectra were also consistent with the simulated results. According to analysis of both simulated and experimental results, modifications in the scanning velocity were capable of adjusting phase shift value. The fabrication method proposed in this paper is simple, convenient, and may be further developed for fabrication of novel tunable fiber filters or DFB fiber lasers.

2. Theoretical modeling and analysis

The proposed phase-shifted FBG is a non-uniform period grating with a discontinuous refractive index distribution. It was formed by introducing the phase shift in a specific area within a conventional FBG, in order to generate two grating segments. The uniform FBG refractive index perturbation was introduced by the interference behind the phase mask and the scanning of the UV laser beam. Hence, the refractive index profile for the phase-shifted FBG is assumed to vary sinusoidally along the fiber direction (i.e. the z direction). This can be expressed as [22]

$$n(z)=n_0+\overline{\delta n_{eff}}(1+\cos(\frac{2\pi}{\Lambda}z+\varphi(z))). \tag{1}$$

Here, n_0 is the refractive index of the fiber core without a perturbation. $\overline{\delta n_{eff}}$ is the average refractive index perturbation in the FBG, which can be considered as the *dc* component of the refractive index change. Λ is the grating period, and $\varphi(z)$ is a function related to the position of the local phase, which is denoted by z.

Optics EXPRESS

Figure 1 presents the refractive index profile for the phase-shifted FBG along the z direction. In this case, the phase-shifted FBG includes the uniform FBG1 and FBG2, which are separated by the shielded section. Generalized couple-mode theory and transfer matrix method [21,22] were used to analyze the transmission properties of the phase-shifted FBG. These proved to be effective for obtaining quantitative information about the spectra of the phase-shifted FBG.

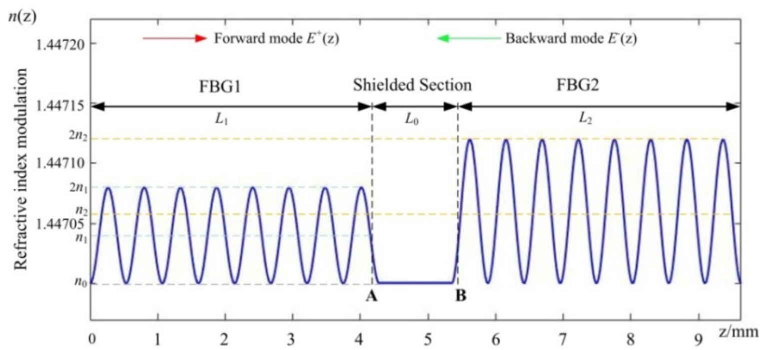

Fig. 1. The refractive index profile of the phase-shifted FBG along the z direction. Note that the grating period has been exaggerated 935 times for clarity.

We assumed the total electric field within the structure to be a sum of the forward E^+(z) and backward E^- (z) propagating modes, traveling in the + z and -z directions, respectively. This can be expressed in terms of the FBG transfer matrix as [23,24]

$$\begin{bmatrix} E^+(0) \\ E^-(0) \end{bmatrix} = [T] \times \begin{bmatrix} E^+(l) \\ E^-(l) \end{bmatrix} = \begin{bmatrix} g & h \\ h^* & g^* \end{bmatrix} \times \begin{bmatrix} E^+(l) \\ E^-(l) \end{bmatrix}, \tag{2}$$

where l is the grating length, and g^* and h^* are the complex conjugates of g and h, respectively. Due to the discontinuities in the refractive index profile, the proposed phase-shifted FBG equals to a short fiber Fabry-Perot cavity, which consists of a pair of FBGs. According to the previous reports [25,26], the effective length of the short fiber Fabry-Perot cavity can be expressed as

$$L_{eff} = L_0 + L_{eff1} + L_{eff2}, \tag{3}$$

where L_0 is the length of the shielded section between two FBGs, L_{eff1} and L_{eff2} are the effective lengths of the left and right FBG (i.e. FBG1 and FBG2), respectively, which can be given by

$$L_{eff1} = L_1 \frac{\sqrt{R_1}}{2a \tanh(\sqrt{R_1})}, L_{eff2} = L_2 \frac{\sqrt{R_2}}{2a \tan h(\sqrt{R_2})}, \tag{4}$$

where L_1, L_2 are the total lengths of FBG1 and FBG2, and R_1, R_2 are the reflectivities of FBG1 and FBG2, respectively. In addition, $R = tanh^2(\pi n_{eff} L/\lambda_B)$, λ_B is the Bragg wavelength.

The equivalent phase-shifted section could be treated as a short fiber Fabry-Perot cavity, and hence we use the effective cavity length L_{eff} to replace the equivalent length of the FBG phase-shifted section. Hence, the transmission matrix of equivalent phase-shifted section can be written as

$$F_p = \begin{bmatrix} e^{i\varphi} & 0 \\ 0 & e^{-i\varphi} \end{bmatrix}, \tag{5}$$

Optics EXPRESS

$$\varphi = \frac{2\pi n_0}{\lambda_B} * L_{eff} = \frac{2\pi n_0 L_0}{\lambda_B} + \frac{n_0 \tan h\left(\pi n_1 L_1 / \lambda_B\right)}{n_1} + \frac{n_0 \tan h\left(\pi n_2 L_2 / \lambda_B\right)}{n_2}. \tag{6}$$

It is obvious from Eq. (6) that the phase shift value φ is determined by the lengths of FBG1, FBG2, and the shielded section (i.e. L_1, L_2, and L_0), and the effective refractive indices of FBG1, FBG2, and the shielded section (i.e. n_1, n_2, and n_0).

Furthermore, the cumulative transmission matrices for the whole phase-shifted FBG can be expressed as

$$\begin{aligned} F &= F_{FBG1} \times F_P \times F_{FBG2} \\ &= \begin{bmatrix} g_1 & h_1 \\ h_1^* & g_1^* \end{bmatrix} \times \begin{bmatrix} e^{i\varphi} & 0 \\ 0 & e^{-i\varphi} \end{bmatrix} \times \begin{bmatrix} g_2 & h_2 \\ h_2^* & g_2^* \end{bmatrix} \\ &= \begin{bmatrix} f_{11} & f_{12} \\ f_{21} & f_{22} \end{bmatrix}. \end{aligned} \tag{7}$$

Finally, the transmission coefficient of the phase-shifted FBG is obtained by imposing the boundary condition $E^-(l) = 0$ [23], and could be expressed as

$$t = \frac{E^+(l)}{E^-(0)}\bigg|_{E^-(l)=0} = \frac{1}{f_{11}}. \tag{8}$$

We used Eq. (8) in the following numerical simulation for obtaining the transmission spectra of the phase-shifted FBG.

3. Experimental setup

A schematic diagram of the phase-shifted FBG inscription process is shown in Fig. 2. First, the single-mode fiber (SMF) was loaded with hydrogen (80°C and 13 MPa for 7 days) to increase the photosensitivity. We used a Corning SMF-28 fiber with a core diameter of 9 µm and a cladding diameter of 125 µm. Secondly, gratings were inscribed in the SMF by a laser source (Coherent, Verdi G-5W) together with a second harmonic generator (SHG, Coherent, model MBD). The Verdi laser generated a CW laser beam at a wavelength of 532 nm. The MBD module generated the second harmonic into an ultraviolet (UV) laser at a wavelength of 266 nm.

The fabrication process can be described in detail as follows: A ~40 mW UV laser with a beam diameter of 3 mm was focused using a cylindrical lens with a focal length of 50.2 mm. The beam was projected through a uniform phase mask (Ibsen Photonics, grating period: 1070 nm, grating area: 50 mm (W) × 10 mm (H)) onto the SMF. In this configuration, the UV laser can produce ± 1 order diffraction beams. The ± 1 order phase mask is optimized to diffract light equally and optimally into ± 1 orders with a 0th order diffraction of less than 1%. Self-interference between the two orders creates an interference pattern with half the phase mask period (i.e. 535 nm). This induced periodic refractive index modulations (i.e. grating generation) when the fiber was exposed to the self-interference section. In this experiment, a homemade plate produced by a UV-proof aluminum foil tape (L_0 ~1.5 mm) was located 2 cm in front of phase mask to shield the fiber from UV laser exposure, as shown in the inset of Fig. 2. The laser focus was adjusted manually to enhance fabrication efficiency during the scanning progress and allow the beam to enter the fiber core. The SMF, with its coating removed, was fixed behind the phase mask at a distance of 300 µm. The phase mask was placed between the cylindrical fiber and the lens to yield a sufficiently periodic intensity pattern along the fiber, which can cause variations in refractive index. The phase mask and fiber were installed on a high-precision translation platform (Newport, M-ILS200PP) and were displaced perpendicular to the focused laser beam. The translation process for the phase

Optics EXPRESS

mask and fiber combination was controlled automatically using LabVIEW software. The uniform FBG1 was inscribed until the UV laser scanned the plate with the scanning velocity v_1, as illustrated in Fig. 2. The effective refractive index of the uniform FBG1 was labeled n_1. Since the fiber was shielded by a plate of length L_0, the refractive index of this shielded section remained constant (i.e. $n(z) = n_0$). Subsequently, the uniform FBG2 with an effective refractive index n_2 was inscribed with a scanning velocity v_2. During the fabrication process, we started to change the scanning velocity v_1 in case the laser beam center reached the left edge of the plate. And then, the scanning velocity was gradually changed into v_2 until the laser beam center reached the right edge of the plate. Transmission spectra were measured simultaneously using a broadband light source (BBS) and an optical spectrum analyzer (Yokagawa AQ6370C) with an intrinsic wavelength resolution of 0.02 nm and a sampling wavelength resolution of 4 pm.

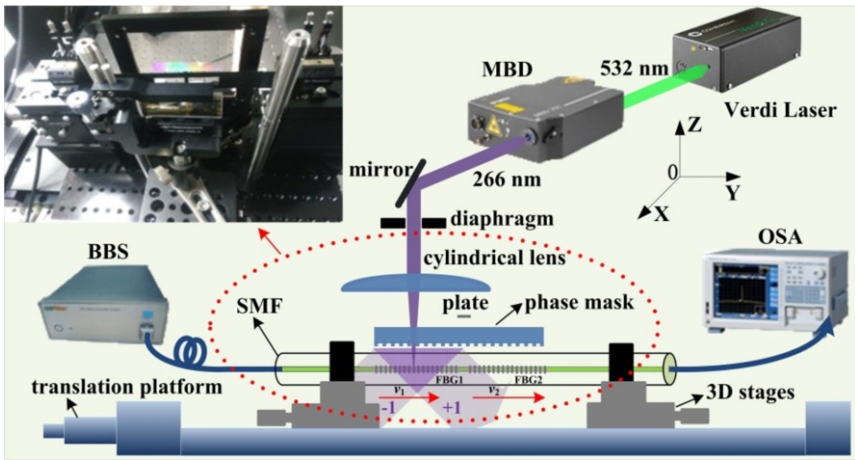

Fig. 2. A schematic diagram of the phase-shifted FBG inscription process.

4. Results and discussion

Figure 3(a) and 3(b) demonstrate the experimental and simulated transmission spectra, respectively, for the uniform FBG1 with scanning length of L_1. In Fig. 3(a), the curves S1-S2 show the evolution of the transmission spectra for the FBG1 with a length of L_1, from 3.33 mm to 20.00 mm. Over this period, the FBG1 with a transmission loss of −14.32 dB was inscribed with a constant scanning velocity v_1 (= 0.050 mm/s). Furthermore, the transmission spectra of the uniform FBG1 were simulated in MATLAB using coupled-mode theory and a transfer matrix method. As illustrated in Fig. 3(b), simulation included a fiber core refractive index of $n_0 = 1.447$, a grating period of $\Lambda = 535$ nm, a center wavelength of $\lambda_B = 1548.97$ nm, and an effective FBG1 refractive index of $n_1 = 1.447 + 5.4e\text{-}5$. The measured results are in good agreement with simulated results.

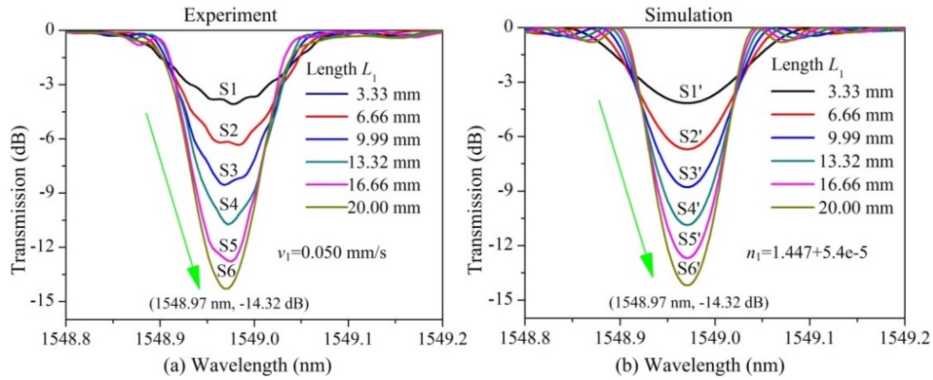

Fig. 3. Experimental and simulated transmission spectra of the uniform FBG1 with various scanning lengths L_1.

t should be noted that the uniform grating refractive index modulation was dependent on velocity, as reported by Legoubin et al. [15]. Namely, the refractive index modulation of the uniform FBG1 and FBG2 was negatively affected by the scanning velocity v_1 and v_2, respectively. In contrast, the refractive index modulation of the uniform FBG1 and FBG2 was positively affected by the laser energy. Based on the above theoretical analysis, the phase shift value φ (i.e. Equation (6)) can be adjusted by scanning velocity, scanning length, and laser energy. In our experiments, the UV laser energy was set to the same value (i.e. 40 mW).

Once the UV laser beam completed scanning the FBG1 at a velocity of v_1, the shielded section (i.e. refractive index of the un-modulated section) was formed by the plate. Finally, the FBG2 was generated gradually at a scanning velocity of v_2. During this time, the transmission spectra evolved gradually from the original FBG to the phase-shifted FBG.

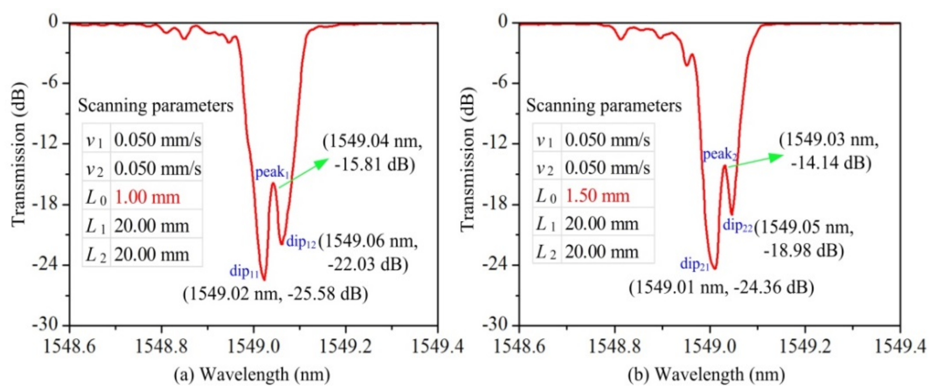

Fig. 4. Transmission spectra of the phase-shifted FBG with various shielded section lengths.

First, two comparable experiments were conducted in which all parameters were set to same values, except for the shielded section length L_0. The transmission spectra of the phase-shifted FBGs with different shielded lengths (L_0) were exhibited in Fig. 4. The scanning parameters in Fig. 4(a) and 4(b), were identical (i.e., $v_1 = v_2 = 0.050$ mm/s, $L_1 = L_2 = 20.0$ mm). The shielded section length (L_0) was 1.00 mm and 1.50 mm in Fig. 4(a) and 4(b), respectively. Differences between the final the transmission spectra of the phase-shifted FBG are evident in these two images (e.g., dip$_{11}$ (−25.58 dB), dip$_{12}$ (−22.03 dB), dip$_{21}$ (−24.36 dB), and dip$_{22}$ (−18.98 dB)). The phase shift value φ is obviously different, and is dependent on the shielded section length L_0 referred to the Eq. (6). However, changing variable shielded section length to adjust phase shift value to a specific value is difficult to control.

Figure 5 demonstrates the experimental and simulated transmission spectra of the phase-shifted FBG with different scanning lengths L_2. In this case, the scanning parameters were set to the following values: v_1 = 0.050 mm/s, L_1 = 20.00 mm, and v_2 = 0.050 mm/s. When the simulations were carried out, as shown in Fig. 5(b), the parameters n_1 and n_2 were first determined by carefully matching the calculated bandwidth and transmission loss at dip wavelength with the experimental results. Subsequently, we gradually changed the phase shift value φ to further match the wavelength of the phase-shifted transmission peak. Hence, we could extract the phase shift values φ from the measured transmission spectra as shown in Fig. 5(a). It is evident from the curves S1-S6 in Fig. 5(a) that the phase shift value φ can be modulated by the scanning length of FBG2 L_2. Curves S1'-S6' in Fig. 5(b) suggest the effective refractive index of the uniform FBG1 and FBG2 to be 1.447 + 5.4e-5. The experimental results are in good agreement with the simulated results except for the peaks of the phase-shifted FBG, which may have been caused by resolution limitation of the optical spectrum analyzer (0.02 nm). Regardless, the simulated results from curve S6' show a −3 dB bandwidth of 3.94 pm in Fig. 5(b). These results illustrate that the different scanning length L_2 can also influence the phase shift value φ, which coincides with the Eq. (6).

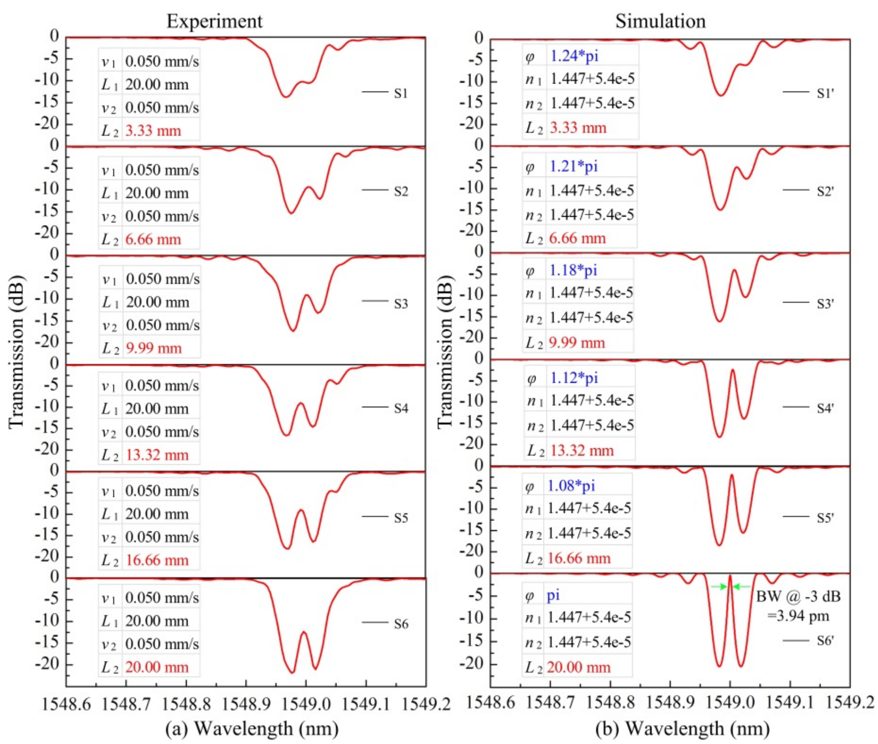

Fig. 5. Experimental and simulated transmission spectra of the phase-shifted FBG with various scanning lengths L_2.

Figure 6 shows the experimental and simulated transmission spectra for the phase-shifted FBG with different scanning velocities v_2. In this case, the scanning parameters were set as follows: v_1 = 0.060 mm/s, L_1 = 20.00 mm, and L_2 = 20.00 mm. The phase shift values φ shown in Fig. 6(b) were extracted from the measured transmission spectra shown in Fig. 6(a) using the same method as described above. It is evident from curves S1-S6 in Fig. 6(a) that the phase shift value φ can be adjusted by changing the scanning velocity v_2. The scanning velocities v_1 and v_2 were set to different values, which can lead to the differences in the refractive index modulation of FBG1 and FBG2. In addition, the phase-shifted FBG fabricated using this method is a new type of optical device, and its characteristics must be

Research Article Vol. 26, No. 10 | 14 May 2018 | OPTICS EXPRESS 13319

further investigated through application to fiber laser sensing. Furthermore, there is an apparent agreement between the experimental and simulated results in Fig. 6(a) and 6(b), which coincide with Eq. (6). The S6 in Fig. 6(a) seems to be distorted comparing to the S6 in Fig. 5(a). This could be explained by the fact that S6 in Fig. 5(a) has a symmetric structure with $L_1 = L_2 = 20$ mm, $v_1 = v_2 = 0.050$ mm/s, whereas S6 in Fig. 6(a) has an asymmetric structure with $L_1 = L_2 = 20$ mm, $v_1 = 0.060$ mm/s, $v_2 = 0.030$ mm/s. The unbalanced grating strengths of FBG1 and FBG2 could lead to a shallower and distorted phase-shifted transmission peak [20].

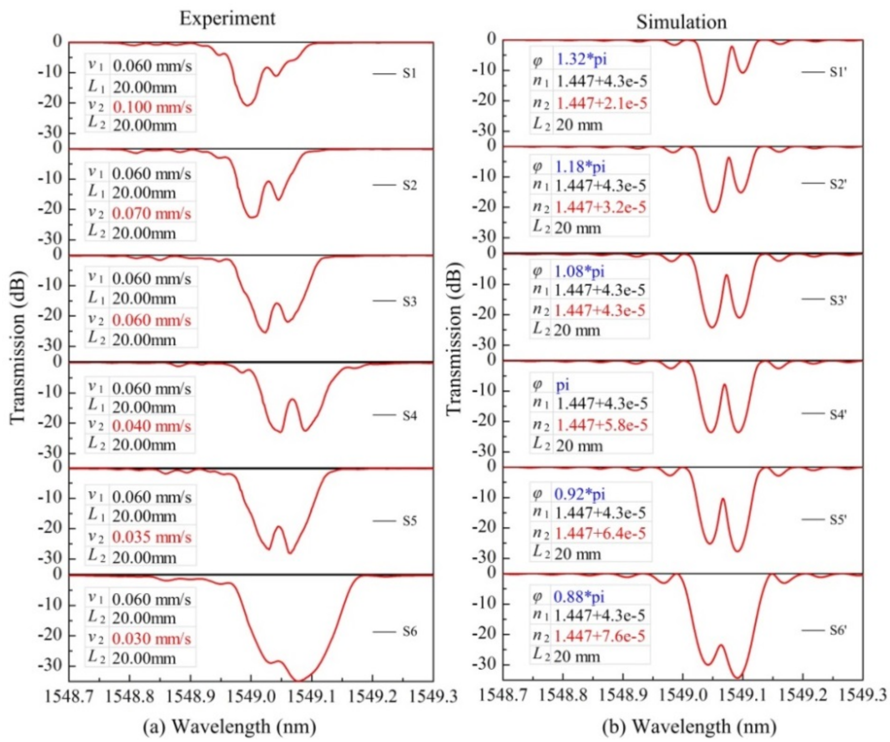

Fig. 6. Experimental and simulated transmission spectra of the phase-shifted FBGs with various scanning velocities v_2.

The variation in the phase shift value φ with scanning length L_2 can be extracted from Fig. 5 and shown in Fig. 7(a), which exhibits a negative linear relationship (black dot) between the phase shift value φ and the scanning length L_2. Additionally, a linear fit (red curve) was obtained with R^2 ~0.96, and a negative slope. Moreover, the variation in the phase shift value φ with the scanning velocity v_2 can be extracted from Fig. 6 and shown in Fig. 7(b), which exhibits a positive linear relationship (black dot) between the phase shift value φ and the scanning velocity v_2. Additionally, a linear fit (red curve) was obtained with R^2 ~0.97, and a positive slope.

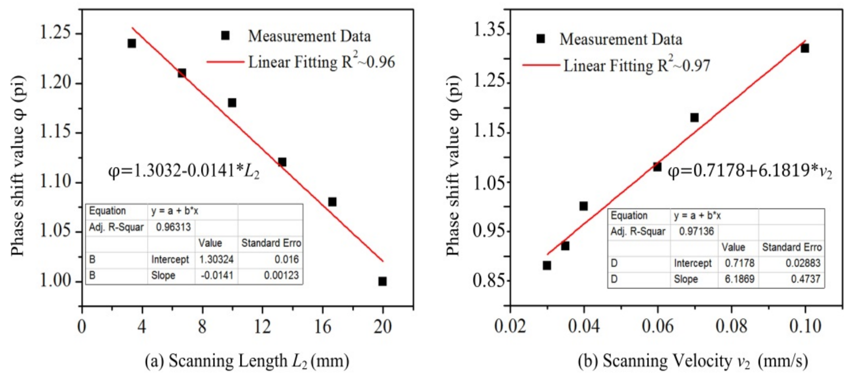

Fig. 7. (a) The variation of phase shift with scanning length L_2. (b) The variation of phase shift with scanning velocity v_2.

As presented in Fig. 8, two π-phase-shifted FBGs with different length proportions (i.e. L_1: L_2) can be fabricated successfully using this method. For Fig. 8(a) and 8(c), the scanning length proportions for FBG1 and FBG2 were 1:1 and 1:2, respectively. In this case, the scanning parameters were set as follows: v_1 = 0.060 mm/s, v_2 = 0.040 mm/s [Fig. 8(a)], v_1 = 0.060 mm/s, and v_2 = 0.034 mm/s [Fig. 8(c)], respectively. The phase-shifted transmission peaks of the fabricated gratings shown in Fig. 8(a) and 8(c) have a FWHM bandwidth (full-width-at-half-maximum, i.e. –3 dB bandwidth) of 16.81 and 16.14 pm, a quality factor Q = 0.011 and 0.012, and a finesse coefficient F = $6.18*10^4$ and $10.01*10^4$, respectively. The parameters Q and F were calculated by the equations Q = FWHM/λ_B and F = $4R/(1-R)^2$, respectively. It seems that decreasing the unbalance in the grating strengths of FBG1 and FBG2 could benefit for improving the finesse of the phase-shifted transmission peaks. In addition, Fig. 8(b) and 8(d) demonstrate the simulated results which are in good agreement with the experimental results. By comparing with the results in Fig. 8(a) and 8(c), a π-phase-shifted FBG with different length proportions can be obtained by adjusting the beam scanning velocity. Consequently, the refractive index modulation of the FBG1 and FBG2 were not the same. These special π-phase-shifted FBGs inscribed in Er-doped fibers could potentially be developed in DFB fiber lasers. The viability of this approach will be investigated further in a future study.

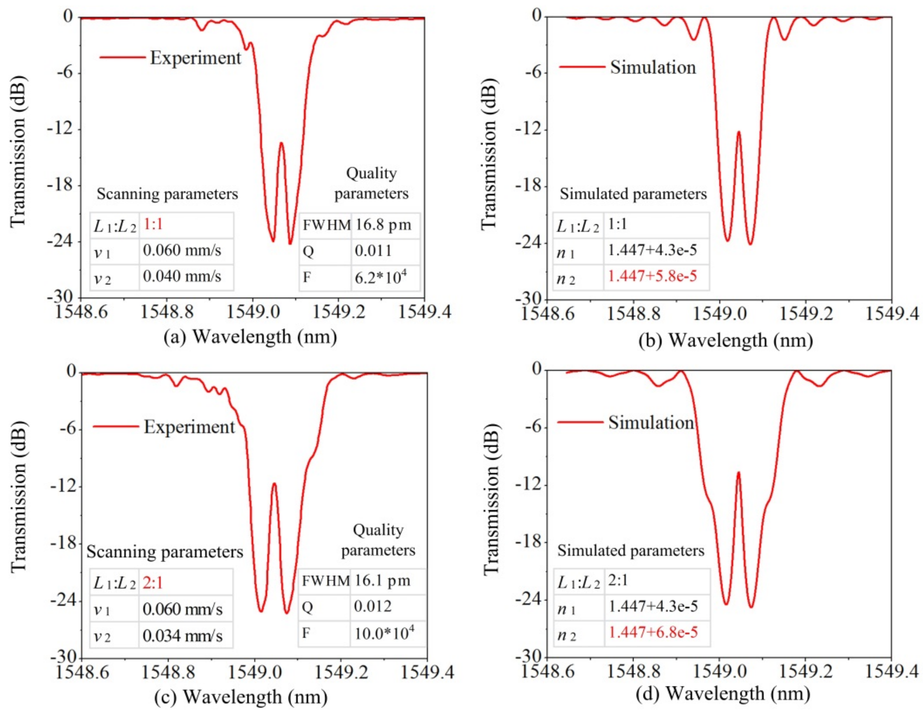

Fig. 8. Experimental and simulated transmission spectra of the phase-shifted FBG with varying length proportions.

5. Conclusion

We have proposed and demonstrated a novel method for fabricating phase-shifted FBGs using a variable velocity scanning UV laser beam in combination with a shielded phase mask. Moreover, we have also analyzed the transmission properties of these phase-shifted FBGs. The experimental results were in good agreement with the simulated results based on coupled-mode theory and a transfer matrix method. The phase shift value of a phase-shifted FBG was found to be dependent on the lengths and effective refractive indices of FBG1, FBG2, and the shielded section. These results illustrate the scanning velocity could adjust the FBG phase shift values and provide a guide for fabricating phase-shifted FBGs using this method. The fabrication process proposed in this paper is simple and convenient. As such, it could be developed further for use in fabricating novel tunable fiber filters or DFB fiber lasers.

Funding

National Natural Science Foundation of China (NSFC) (grants 61505120, 61425007, 61635007); Guangdong Natural Science Foundation (grants 2017A010102015, 2015A030310243, 2015B010105007, 2014A030308007); Science and Technology Innovation Commission of Shenzhen(grants JCYJ20170302143105991, JCYJ20170412105604705, JCYJ20160427104925452, JCYJ20170302154614941, JCYJ20160307143716576); Development and Reform Commission of Shenzhen Municipality Foundation.